Insect Biochemistry and Molecular Biology 119 (2020) 103315

Contents lists available at ScienceDirect

Insect Biochemistry and Molecular Biology

journal homepage: www.elsevier.com/locate/ibmb

Excess melanin precursors rescue defective cuticular traits in *stony* mutant silkworms probably by upregulating four genes encoding RR1-type larval cuticular proteins

Liang Qiao[b,1,*], Zheng-wen Yan[a,1], Gao Xiong[a], You-jin Hao[b], Ri-xin Wang[a], Hai Hu[a], Jiang-bo Song[a], Xiao-ling Tong[a], Lin-rong Che[b], Song-zhen He[a], Bin Chen[b], James Mallet[c], Cheng Lu[a], Fang-yin Dai[a,**]

[a] State Key Laboratory of Silkworm Genome Biology, Key Laboratory of Sericultural Biology and Genetic Breeding, Ministry of Agriculture and Rural Affairs, College of Biotechnology, Southwest University, Chongqing 400715, China
[b] Chongqing Key Laboratory of Vector Insects, Institute of Entomology and Molecular Biology, College of Life Sciences, Chongqing Normal University, Chongqing, 401331, China
[c] Department of Organismic and Evolutionary Biology, Harvard University, Cambridge, MA 02138, USA

ARTICLE INFO

Keywords:
Melanic coloring
Cuticle features
Cuticular protein-encoding genes
Induction
Bombyx mori

ABSTRACT

Melanin and cuticular proteins are vital cuticle components in insects. Cuticular defects caused by mutations in cuticular protein-encoding genes can obstruct melanin deposition. The effects of changes in melanin on the expression of cuticular protein-encoding genes, the cuticular and morphological traits, and the origins of these effects are unknown. We found that the cuticular physical characteristics and the expression patterns of larval cuticular protein-encoding genes markedly differed between the melanic and non-melanic integument regions. By using four *p* multiple-allele color pattern mutants with increasing degrees of melanism ($+^{p}$, p^{M}, p^{S}, and p^{B}), we found that the degree of melanism and the expression of four RR1-type larval cuticular protein-encoding genes (*BmCPR2*, *BmLcp18*, *BmLcp22*, and *BmLcp30*) were positively correlated. By modulating the content of melanin precursors and the expression of cuticular protein-encoding genes in cells in tissues and *in vivo*, we showed that this positive correlation was due to the induction of melanin precursors. More importantly, the melanism trait introduced into the *BmCPR2* deletion strain Dazao-*stony* induced up-regulation of three other similar chitin-binding characteristic larval cuticular protein-encoding genes, thus rescuing the cuticular, morphological and adaptability defects of the Dazao-*stony* strain. This rescue ability increased with increasing melanism levels. This is the first study reporting the induction of cuticular protein-encoding genes by melanin and the biological importance of this induction in affecting the physiological characteristics of the cuticle.

1. Introduction

Melanic color patterns play important roles in many adaptive processes in insects, such as mimicry, mating preference, and the ability to resist pathogens and UV thermoregulation (Hu et al., 2013; Liu et al., 2015a; Mallet and Hoekstra, 2016; True, 2003; Wilson et al., 2001; Wittkopp et al., 2003).

The roles of melanism in insects rely on not only the integrity of melanin biosynthesis and regulatory pathways (Futahashi and Fujiwara, 2005; Wittkopp and Beldade, 2009; Wittkopp et al., 2003) but also the presence of the 'platform' on which melanin relies (Andersen, 2010; Moussian, 2010; Van Belleghem et al., 2017; Wittkopp and Beldade, 2009; Wittkopp et al., 2003). In insects, the cuticle is the most important platform for the formation of the melanic color pattern (Andersen, 2010; Hopkins and Kramer, 1992; Moussian, 2010). During the shaping of the cuticle, the maintenance of the cuticle's features depends on cuticular proteins and their interactions with other components (Andersen, 2010; Chaudhari et al., 2011; Guan et al.,

* Corresponding author. Chongqing Key Laboratory of Vector Insects, Institute of Entomology and Molecular Biology, College of Life Sciences, Chongqing Normal University, Chongqing, 401331, China.
** Corresponding author. State Key Laboratory of Silkworm Genome Biology, Key Laboratory of Sericultural Biology and Genetic Breeding, Ministry of Agriculture and Rural Affairs, College of Biotechnology, Southwest University, Chongqing 400715, China.
E-mail addresses: qiaoliangswu@163.com (L. Qiao), fydai@swu.edu.cn (F.-y. Dai).
[1] Equally contributed.

https://doi.org/10.1016/j.ibmb.2020.103315
Received 7 March 2019; Received in revised form 3 January 2020; Accepted 8 January 2020
Available online 13 January 2020

2006; Hopkins and Kramer, 1992; Moussian, 2010; Noh et al., 2016; Suderman et al., 2006).

Because of the critical roles of cuticular proteins in cuticle development, if the genes including these proteins lose their functions, the defective cuticle affects the deposition and attachment of melanin, thereby influencing the formation of the melanic color pattern (Arakane et al., 2012; Kanekatsu et al., 1988; Noh et al., 2015; Oota and Kanekatsu, 1993; Xiong et al., 2017). Little is known about how cuticular protein-encoding genes respond to alterations in melanin biosynthesis or regulatory pathways.

Recently, several reports have shown that the abundance of cuticular protein-encoding genes in different colored integuments varies in insect species, and that these genes are up-regulated in the melanic cuticle regions (Futahashi et al., 2012; He et al., 2016; Jan et al., 2017; Wu et al., 2016). Some of those cuticular protein-encoding genes have similar expression patterns and functions (Liang et al., 2010; Nakato et al., 1994, 1997; Okamoto et al., 2008; Qiao et al., 2014; Shofuda et al., 1999; Tang et al., 2010). These studies suggest a likely relationship between the promotion of melanism and the expression of cuticular protein-encoding genes. Prior to this study, the potential relationships among cuticular protein-encoding genes were unclear. Additionally, when melanism signaling and defects in cuticle proteins occur simultaneously, the net effects on the morphological and physiological traits are also unclear.

In the Lepidoptera model *Bombyx mori*, an intriguing phenomenon has been reported in which the larval melanic mutant *Striped* (p^S, 2–0.0) reverses the malformed body shape and the adaptability defects of the *stony* mutant (*st*, 8–0.0) (Dai et al., 2000; Xiang, 1995). A recent study has reported that the transcription factor *Apontic-like*, which increases the expression of melanin synthesis genes in epidermal cells, is responsible for the p^S mutant phenotype (Yoda et al., 2014). Multiple alleles exist with different degrees of melanism at the *p* locus, including p^B and p^M (Banno et al., 2005; Xiang, 1995; Yoda et al., 2014). The *stony* mutant (*st*, 8–0.0) is caused by a deletion of a portion of a RR1-type larval cuticular protein-encoding gene *BmCPR2* (*BmLcp17*). The *stony* mutant has is hard and tight to the touch, and has imbalanced ratios of the lengths of the internodes (I) and the intersegment folds (IF) (I/IF of approximately 1.6 in the *stony* mutation and approximately 4 in the wild-type strain), bulges at the intersegment folds, and severely altered locomotion and behavioral activities in the larval stage (Qiao et al., 2014). The similarities in the gene expression patterns (Fig. S1) and functional characteristics of the other RR1-type larval cuticular protein-encoding genes (*Lcps*), *BmLcp18*, *BmLcp22*, and *BmLcp30* also suggest that they may play very similar roles to those of *BmorCPR2* in shaping the larvae cuticle (Dong et al., 2016; Liang et al., 2010; Nakato et al., 1994, 1997; Okamoto et al., 2008; Qiao et al., 2014; Shofuda et al., 1999; Tang et al., 2010). These findings can be linked through the epistasis of p^S to *stony* (Dai et al., 2000), and provide highly useful genetic resources for exploring the interactions between melanin and cuticular protein-encoding genes.

In the present study, we found that the transcript levels of *BmorCPR2*, *BmLcp18*, *BmLcp22*, and *BmLcp30* were positively correlated with the degree of melanism of the larval cuticle. This positive correlation was due to the simultaneous induction of these genes by melanin precursors. Moreover, after melanism induction in the *stony* mutant, the cuticle deficiency was rescued through functionally similar compensation by up-regulated *BmLcp18*, *BmLcp22*, and *BmLcp30*. These findings provide new evidence indicating that melanism is a beneficial trait and also deepen understanding of the interactions among the genetic factors shaping morphological features in Lepidopterans.

2. Materials and methods

2.1. Silkworm strains

The wild-type strain Dazao ($+^p$) and melanic mutant strains p^M, p^S, and p^B (Banno et al., 2005; Xiang, 1995; Yoda et al., 2014) were used in this study. The pigment intensity was measured as the mean OD value in Image J (https://imagej.nih.gov/ij/). In terms of the degree of melanism, the body color of an individual homozygous at the p^M or p^S loci is darker than that of a heterozygous individual (Banno et al., 2005; Xiang, 1995). The albinism mutant *albino* (*al*) (Banno et al., 2005; Fujii et al., 2013), the non-diapause wild-type strain N4 (used for melanin inhibition treatment), the *BmCPR2* deletion strain, and the Dazao-*stony* strain (a near isogeneic line of Dazao, which has been backcrossed with Dazao for more than 26 generations) were supplied by the Silkworm Gene Bank at Southwest University. The N4 strain and *al* mutant were fed an artificial diet at 28 °C. All other strains were fed fresh mulberry leaves under a 12 h/12 h light/dark photoperiod at 24 °C.

2.2. Chemicals and cell lines

L-Dopa, dopamine, tetrahydrofolic acid (BH_4, a cofactor for the synthesis of melanin), and 2,4-diamino-6-hydroxypyrimidine (DAHP, an inhibitor of guanylate cyclase hydrolase (GTPCHI), an important rate-limiting enzyme in the synthesis of BH_4 (Delgado-Esteban et al., 2002; Mitchell et al., 2003) in melanin metabolism) were purchased from Sigma-Aldrich (St. Louis, MO, USA). The *Bombyx mori* embryonic (*BmE*) cell line was established in our laboratory more than 10 years ago and was used for the basal expression analysis of *BmCPR2*, *BmLcp18*, *BmLcp22*, *BmLcp30*, and *BmCPH24* (Fig. S2).

2.3. Chitin content determination

Melanic and non-melanic larval cuticles were dissected, and the attached tissues were also removed; samples were then washed with double distilled H_2O and dried at 60 °C. Dried cuticles were weighted with an analytical balance (METTLER-MS105DU, Germany). The extraction and determination of chitin content were conducted as described by Kunyan Zhu et al. (Zhang and Zhu, 2006) with slight modifications. Three or four biological replicates for each sample were examined.

2.4. Scanning electron microscopic analysis

Melanic and non-melanic larval cuticles were dissected, and the attached tissues were also removed; samples were then washed with double distilled H_2O and gradually dehydrated according to Hu's method (Hu et al., 2009). Samples were sputter-coated with gold with a Hitachi E−1010 high-resolution sputter coater (Hitachi, Japan) and observed under a Hitachi S–3000N scanning electron microscope (Hitachi, Tokyo, Japan).

2.5. Mating combinations and progeny phenotype identification

The p^S and p^M strains were crossed with the Dazao-*stony* strain to generate the F_1 generation. The F_2 generation was produced by F_1 self-crossing F_1. Individuals at day 5 of the 5th instar (the larval stage is approximately 8 days in the experimental conditions of our laboratory) of F_2 were collected for further use. The p^B strain was crossed with the Dazao-*stony* strain to generate F_1 progeny, which were then mated with the Dazao-*stony* strain to generate the BC_1 generation. The BC_1 generation was fed until day 5 of the 5th instar.

Individuals of the F_2 or BC_1 generations were separated according to cuticle pigmentation. Subsequently, phenotypes were classified by morphological characteristics, and I/IF ratios in the second, third, and fourth abdominal segments, according to a previously described method (Qiao et al., 2014).

2.6. Genotyping

Because the p^S, p^M, and p^B mutations are alleles at the *p* locus, they

should be located in proximity on chromosome 2 (Banno et al., 2005; Xiang, 1995; Yoda et al., 2014). According to the gene sequence of the p^S allele, 11 PCR primer pairs in a 12.4 kb genomic region (from 3.9 kb upstream of the translation initiation site (ATG) of *apt-like* to 8.5 kb downstream of the initial codon) were used. PCR screening was performed for p^M, p^S, p^B, and the Dazao-*stony* strain to obtain molecular markers of polymorphism for the *p* locus. We found a molecular marker at 1.47 kb (within the intron region) downstream of the initial codon. Similarly, a PCR-based molecular marker was also designed within genomic region of *BmCPR2* to screen for polymorphism at the *stony* locus, and the primers were used to analyze CDS sequence differences between *stony* and wild-type as in our previous study (Qiao et al., 2014). The primers used in this study are listed in Table S1.

2.7. Analysis of phenotype, genotype, and gene expression

Day 5 5th instar larvae of the Dazao and Dazao-*stony* strains (the larval stage is approximately 8 days in the experimental conditions of our laboratory) were selected for cuticle dissection. The cuticles of the semi-lunar marking region and the non-melanic portion between the paired semi-lunar markings were dissected. Gene expression levels of *BmCPR2* (KF672849.1), *BmLcp18* (NW_004582021.1), *BmLcp22* (NW_004582025.1), *BmLcp30* (NW_004582025.1), *BmCPR68* (NM_001173219), *BmCPR3* (NM_001173273), *BmCPR129* (NM_001173170), *BmCPG13* (NM_001173319), *BmCPH25* (NM_001173281), *Bmyellow* (DQ358085.2), *BmDDC* (NW_004582031.1), and *Bmlaccase 2* (NW_004582017.1) in these regions were compared. Gene expression patterns were determined for the dorsal epidermis of abdominal segments (from semi-lunar marking to star marking) from day 5 5th instar larvae of Dazao, $p^S/+$, $p^M/+$, and $p^B/+$ strains. The 2nd instar larvae at day 1 were also analyzed in the *al* and Dazao strains. The dorsal epidermis regions (from the semi-lunar marking to the star marking) were collected from the BC_1 and F_2-generation of the $p^B/+^{pB}$, $+^{st}/st$, $p^B/+^{pB}$, *st/st*, p^S/p^S, *st/st*, $p^S/+^{pS}$, *st/st*, p^M/p^M, *st/st* and $p^M/+^{pM}$, and *st/st* genotypes for gene expression analysis. For all genotyped individuals, the I/IF ratios were also analyzed in Image J (https://imagej.en.softonic.com/).

2.8. Confocal microscopy analysis

The cuticles of day 5 5th instar larvae (strains: p^S, Dazao, Dazao-*stony*, and $p^B/+^{pB}$, +*st/st*, $p^B/+p^B$, *st/st*, p^S/p^S, *st/st*, $p^S/+^{pS}$, *st/st*, p^M/p^M, *st/st*, $p^M/+^{pM}$, *st/st*, $+^P/+^P$, and *st/st* in BC_1 and cross F_2 progeny) were dissected. After removal of attached tissues, such as the dermis and muscles, the cuticle was washed for 5 min in 1 × PBS buffer and fixed in 4% paraformaldehyde for 1 h at 4 °C. After being washed three times in 1 × PBS (5 min each time), the cuticles were air-dried and embedded in embedding agent (SAKURA Tissue-Tek O.C.T compound, USA) for 30 min at −20 °C. Then 4 μm slices were prepared on a HM525 NX freezing microtome (Thermo Scientific, USA). Confocal imaging was performed with a FV3000 (OLYMPUS, Japan) confocal microscope (objective lens: 60 × , zoom: 1.67 ×) and then merged in Z-Dimension mode. The cuticle thickness was measured with Image J (https://imagej.en.softonic.com/). Three biological replicates were examined for each sample, and more than three observations were made for repeat samples.

2.9. Melanin precursor promoting and inhibiting treatments

L-Dopa and dopamine solutions were prepared according to Futahashi, with slight modifications (Futahashi and Fujiwara, 2005). L-Dopa and dopamine solutions were filtered with 0.22 μm membranes before use. *BmE* cells were washed three times with Grace medium without melanin precursors to remove metabolites and other contaminants on the cell surfaces. Medium (0.8 mL) containing L-Dopa or dopamine was added separately into each well of a 24-well plate. Medium without melanin precursors was used as a control for gene expression analysis. Culture plates were sealed with tape, wrapped with foil, and incubated at 28 °C for 24 h for gene expression analysis. For BH_4 feeding assays, a 30 mM working solution was prepared by dissolving tetrahydrofolic acid into double distilled H_2O and spreading it on an artificial diet for the *al* mutant strain. As a control, the *al* mutant strain (with albinism and a porous cuticle, owing to a mutation in the sepiapterin reductase gene, which leads to insufficient synthesis of the cofactor BH_4 during the synthesis of melanin precursors (Banno et al., 2005; Fujii et al., 2013)), fed with an artificial diet treated only with double distilled H_2O, was used. Phenotypes were recorded from the 2nd instar stage, and expression of cuticular protein-encoding genes was analyzed.

To perform the melanism-inhibition experiments, we used the wild-type strain N4 (melanic body color at 2nd instar stage). Newly hatched larvae were divided into treatment and control groups. Individuals in the treatment group were fed an artificial diet containing DAHP (dissolved in 0.1 M NaOH), and individuals in the control group were fed an artificial diet containing 0.1 M NaOH.

To prepare artificial diets with or without DAHP, the following procedures were performed: for the treatment group, 2.5 g DAHP was dissolved in 0.1 M NaOH (with a total volume of 150 mL); then 50 g artificial food was added and mixed in, and the diet was further treated at 98 °C for 25 min. For the control group, although no DAHP was added, the other treatment procedures were the same. The larvae were separately fed artificial feed once daily for three consecutive days. The day 1 2nd instar larvae were selected for phenotype and expression analysis.

2.10. Integument culture

The procedures for integument cultures were carried out according to Futahashi and Fujiwara (2006) with minor modifications. The Dazao strain at day 5 5th instar was selected to dissect the non-melanic integuments on the dorsal side of the 3rd–4th abdominal segments. After removal of the muscle, trachea, and fat body, the tissues were cut into rectangles (4 mm × 4 mm), washed five times in 1 × PBS, and dried on sterile filter paper. Three to six pieces of integuments were placed in 1.5 ml microcentrifuge tubes, and 600 μl Grace medium (GIBCO BRL) was added, including 6 μg/ml phenylthiourea (to prevent phenol oxidase activity), penicillin-streptomycin (100 U/ml), streptomycin (0.1 mg/ml), and 5 mM L-Dopa or dopamine. The mixture was gently stirred to disperse the integuments, sealed to avoid light, and then placed on a shaker and incubated at 24 °C for 24 h at a speed of 80 rpm/min (with the angle not exceeding 30° during incubation). Grace medium without L-Dopa and dopamine was used as the control. After incubation, the dermal cell layers on the integuments were gently scraped off and washed with 1 × PBS. The degree of melanism in the cuticle was determined under a stereomicroscope (OLYMPUS, Japan). Gene expression patterns were detected by quantitative reverse transcription-PCR (qRT-PCR). Phenotypic observations and gene expression detection in the treatment group and control group were performed on at least three biological replicates.

2.11. Overexpression of BmCPH24

Overexpression vectors for *BmCHP24* (larval cuticular protein-encoding genes) and *piggyBac* (*A3*-EGFP, *IE1-BmCPH24-SV40*) were constructed in our laboratory by Xiong et al. (2017). The empty vector without *BmCPH24* was used as a control. One microgram of overexpression vector and control vector were transfected into *BmE* cells with X-tremeGENE HP (Roche, Basel, Switzerland). Two days post-transfection, transfected cells were observed, and cells with high fluorescence intensity were collected for RNA extraction. The expression of cuticular protein genes in overexpression cells and controls was determined with qRT-PCR. Primers are listed in Table S1.

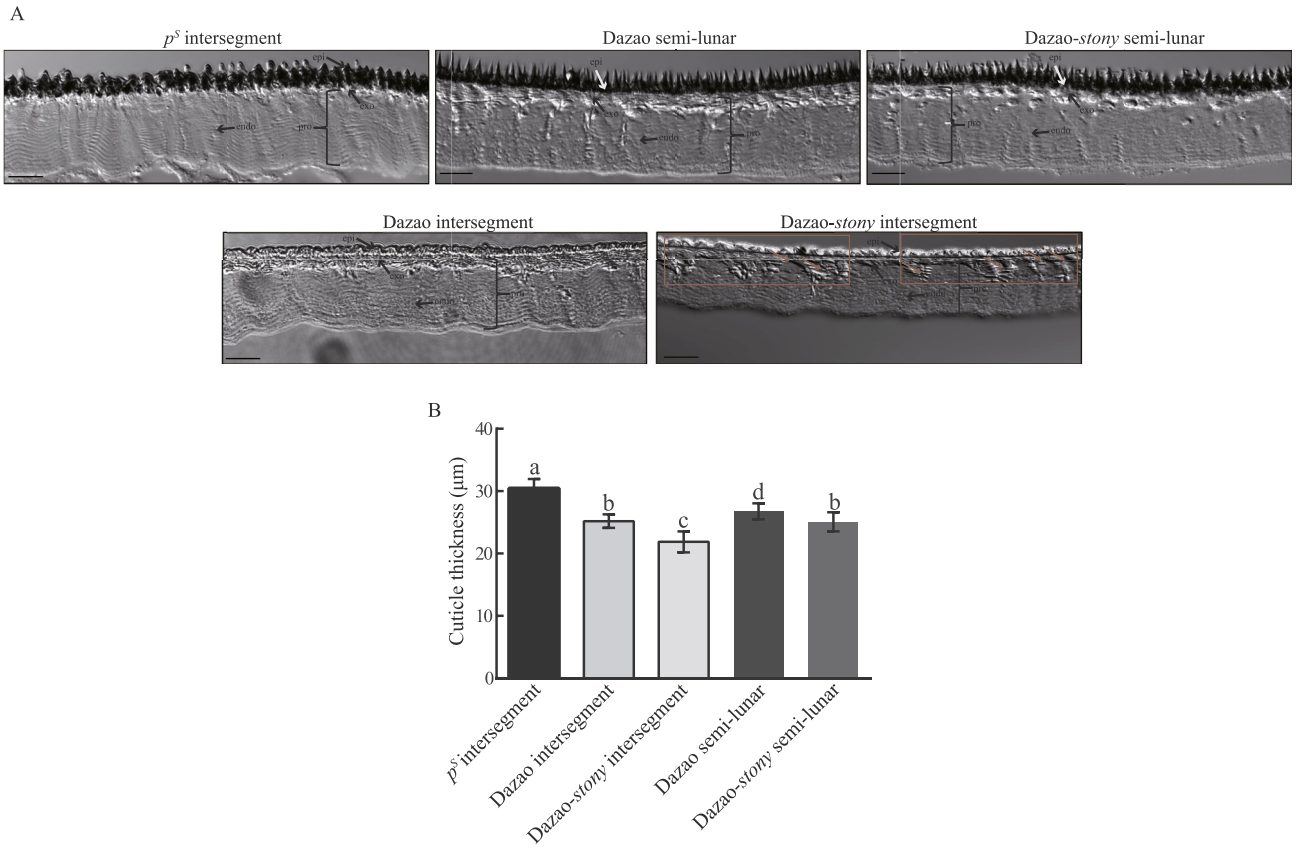

Fig. 1. Comparison of the physical structure between melanic and non-melanic cuticle. A. Cross-section of cuticle from the same integument areas in Dazao, Dazao-*stony*, and p^S. Scale bar = 10 μm. Epi: epicuticle, exo: exocuticle, endo: endocuticle, pro: procuticle. The disordered arrangements in the procuticle of Dazao-*stony* are boxed in red. Red arrows indicate damage to the exocuticle in Dazao-*stony*. B. Thickness of cuticles in Figure A. One-way ANOVA test, n = 3, F = 47.36, n = 3, $p < 0.05$. (For interpretation of the references to color in this figure legend, the reader is referred to the Web version of this article.)

2.12. Quantitative RT–PCR

Total RNA extraction, reverse transcription, and qRT-PCR were performed as described previously (Qiao et al., 2014). Three biological replicates were prepared for each condition, and the house-keeping gene *BmRPL3* was used as the internal control. Primers used are listed in Table S1.

3. Results

3.1. Cuticle physical characteristics are entirely distinct between melanic and non-melanic cuticular regions

The cuticle section slices showed that the melanin protrusions were deposited in the epicuticle of the p^S strain and the lunar marking of the Dazao strain (Fig. 1A). The thickness of the melanic cuticle was also greater than that of the non-melanic cuticle (Fig. 1B). Moreover, the surface nanostructures were much denser in the melanic regions than in the non-melanic regions, regardless of strain (Fig. S3A), owing to the deposition of melanin in the epicuticle. The content of chitin (a major component for cuticle construction, which is closely related to cuticle pigmentation (Moussian et al., 2005; Moussian et al., 2006)) was correspondingly increased in the melanic cuticle (Fig. S3B). In non-melanic regions of the *stony* mutant, the arrangement of the procuticle was disordered, and damage to the exocuticle was observed (Fig. 1A). The intersegments cuticle of the stony mutant was the thinnest relative to that in the intersegments cuticles of p^S, Dazao, and the semi-lunar marking cuticular region of Dazao and Dazao-*stony* (Fig. 1B). However, the disordered arrangement of the procuticle in the melanic semi-lunar marking region of the *stony* mutant was not observed (Fig. 1A). The cuticle was also thicker than that in the non-melanic region of the Dazao-*stony* strain (Fig. 1B).

3.2. Correlation of larval cuticular protein-encoding gene expression with cuticle melanism

The expression levels of *BmCPR2*, *BmLcp18*, *BmLcp22*, and *BmLcp30* were higher in the melanic regions than the non-melanic regions (Fig. 2). We further investigated the expression patterns of those genes by using four alleles of the *p* locus (Dazao ($+^p$), p^M, p^S, and p^B) with greater melanin accumulation than that in the Dazao strain (Fig. 3A). Expression levels of *BmorCPR2*, *BmLcp18*, *BmLcp22*, and *BmLcp30* were gradually and up-regulated with increasing melanism in the cuticle (Fig. 3B, Fig. S4). These results showed that the expression of *BmorCPR2*, *BmLcp18*, *BmLcp22*, and *BmLcp30* correlated positively with the degree of melanism (Fig. 3, Fig. S4).

3.3. Effects of melanin precursors on the expression of cuticular protein-encoding genes

The basal expression of four larval cuticular protein-encoding genes was analyzed in *BmE* cells (Fig. S2), thus indicating that regulatory pathways controlling the expression of these cuticular protein-coding genes were present in this cell line. After incubation of *BmE* cells with melanin precursors, the expression of cuticular protein-encoding genes was higher in cells treated with either L-Dopa or dopamine than in the control cells (Fig. 4A). In addition, when the 2nd instar *al* mutant was treated with BH_4, the larvae had a normal melanic body color (Fujii et al., 2013), and the expression of four RR1-type *BmLcps* was higher than in the control group (Fig. 4B). Moreover, in the wild-type 2nd

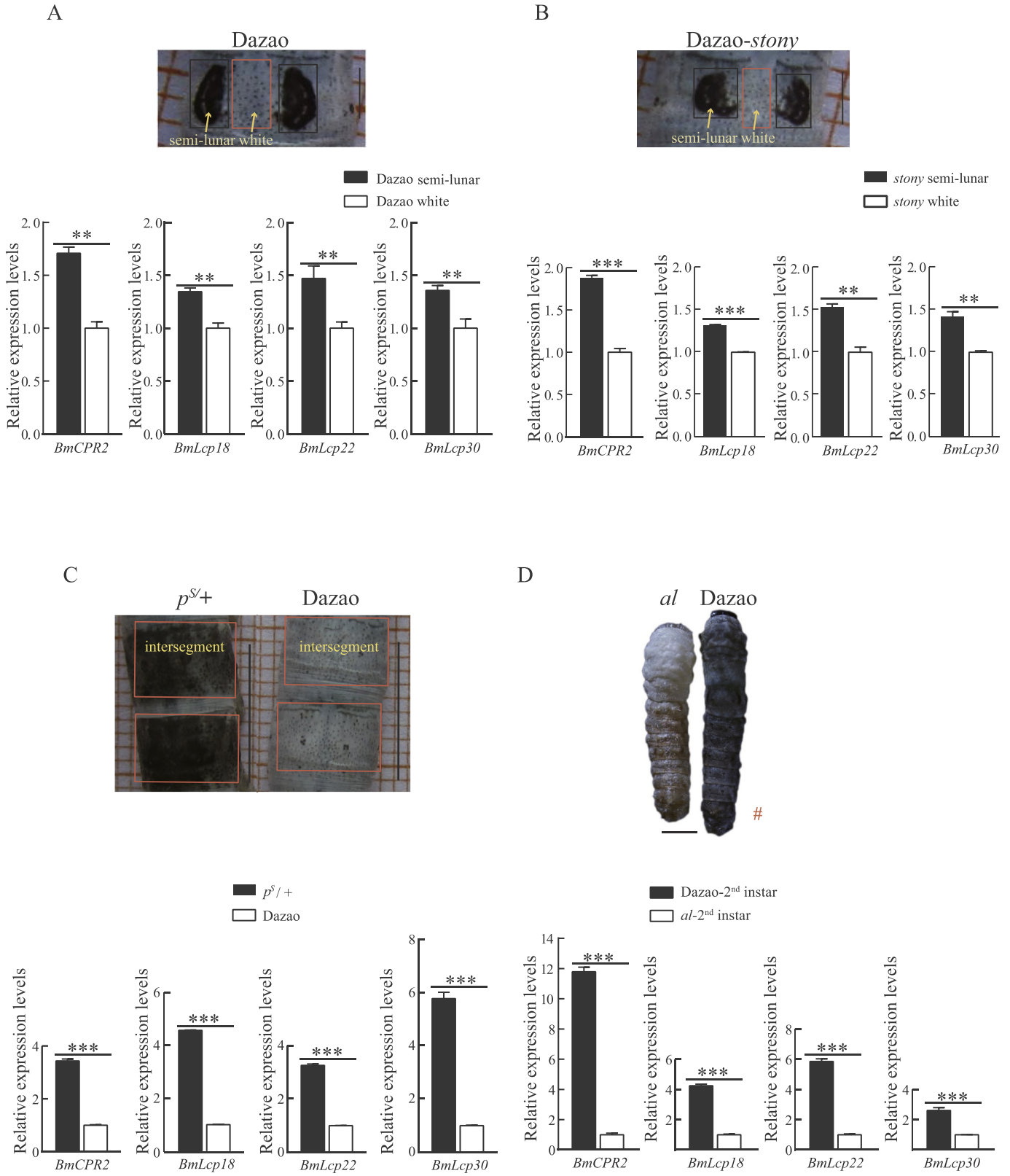

Fig. 2. Expression of *BmCPR2*, *BmLcp18*, *BmLcp22*, and *BmLcp30* in melanic and non-melanic integuments. A and B show relative gene expression levels in the semi-lunar marking (black box) and the non-melanic region (between the semi-lunar marking, red box) in Dazao and Dazao-*stony* strains. Scale bar is 2 mm. C shows a comparative analysis of relative gene expression levels at the dorsal side of abdominal segments (from the third to the fourth segment, red box) in p^S and Dazao strains. Scale bar is 1 cm. D shows a comparison of relative gene expression levels between the 2nd instar *al* mutant and the Dazao strain (melanic). The red hash tag symbol indicates that the Fig. 1 D shown here is from a previous study from our group (Min et al., 2016) with modifications. Scale bar is 2 mm n = 3, *t*-test, asterisks denote statistical significance, $*p < 0.05$; $**p < 0.01$; $***p < 0.001$.

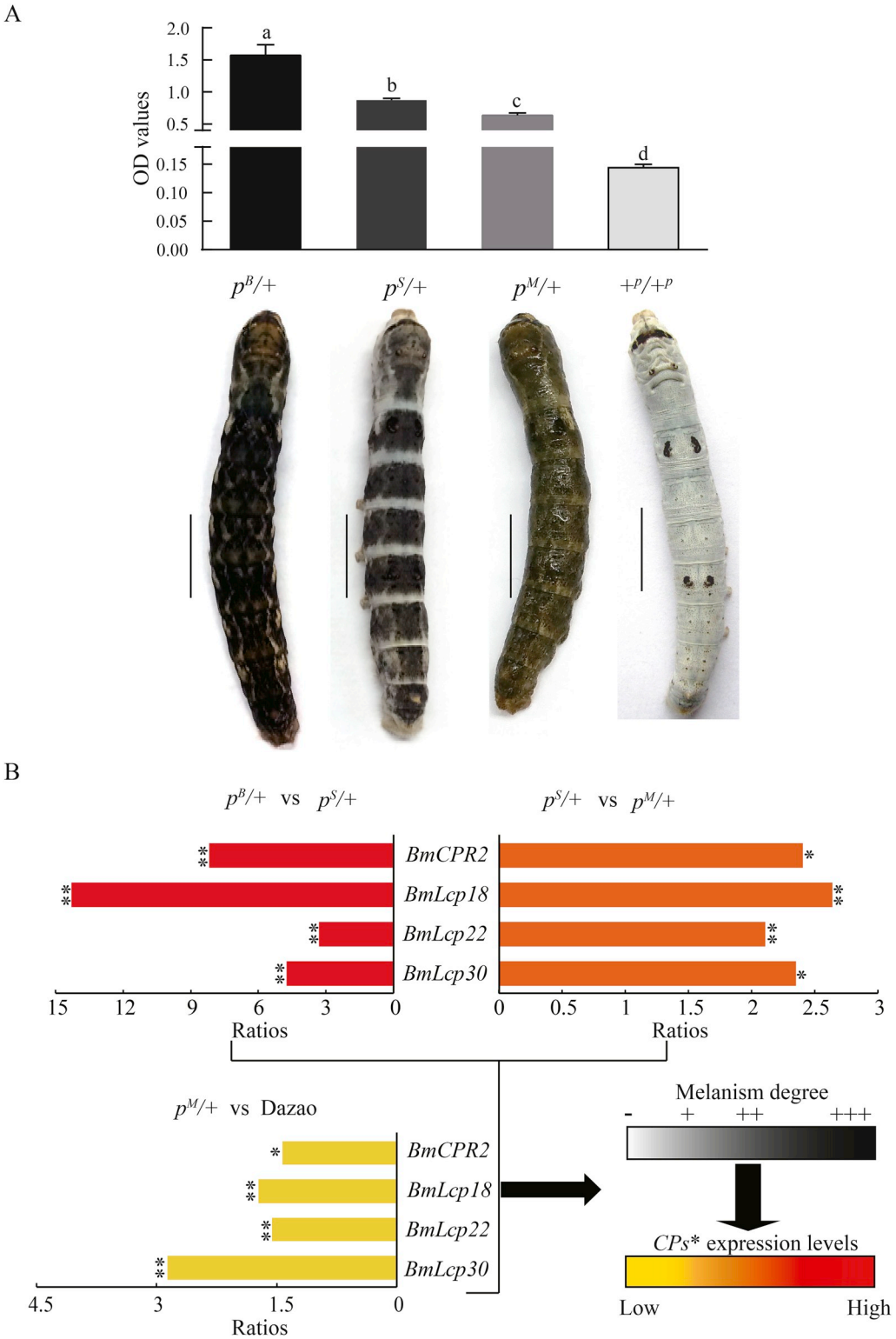

Fig. 3. Expression of cuticular protein-encoding genes in integuments with different degrees of melanism. A. Comparison of melanism degree. One-way ANOVA test, n = 6, F = 290.6, $p < 0.0001$. B. Gene expression levels of cuticular protein-encoding genes among four strains with mutant alleles at the *p* locus ($+^p$, p^M, p^S, and p^B). Scale bar is 1 cm. Ratios represent the ratios of gene expression levels between two strains. Symbols (−, +, + +, and + + +) represent the degree of melanism. Stars represent melanin-associated cuticular protein-encoding genes. *t*-test, n = 3, asterisks denote statistical significance, $*p < 0.05$; $**p < 0.01$.

instar larvae treated with DAHP, the cuticles lost their original melanic body color (Tong et al., 2018), and the expression of four RR1-type *Bm Lcps* was lower than that in the control group (Fig. 4C). Furthermore, regarding the unchanged melanin precursor content, the expression of *BmLcp18*, *BmLcp22*, and *BmLcp30* was not affected by the deletion of *BmLcp17* (Fig. S5). The larval cuticular protein-encoding gene *BmCPH24* (with a similar expression pattern to those of the four RR1-type *BmLcps*. Loss of function of *BmCPH24* also produced a *stony*-like phenotype, but with more pronounced defects (Xiong et al., 2017)) was overexpressed, yet had no effect on the expression of the four RR1-type

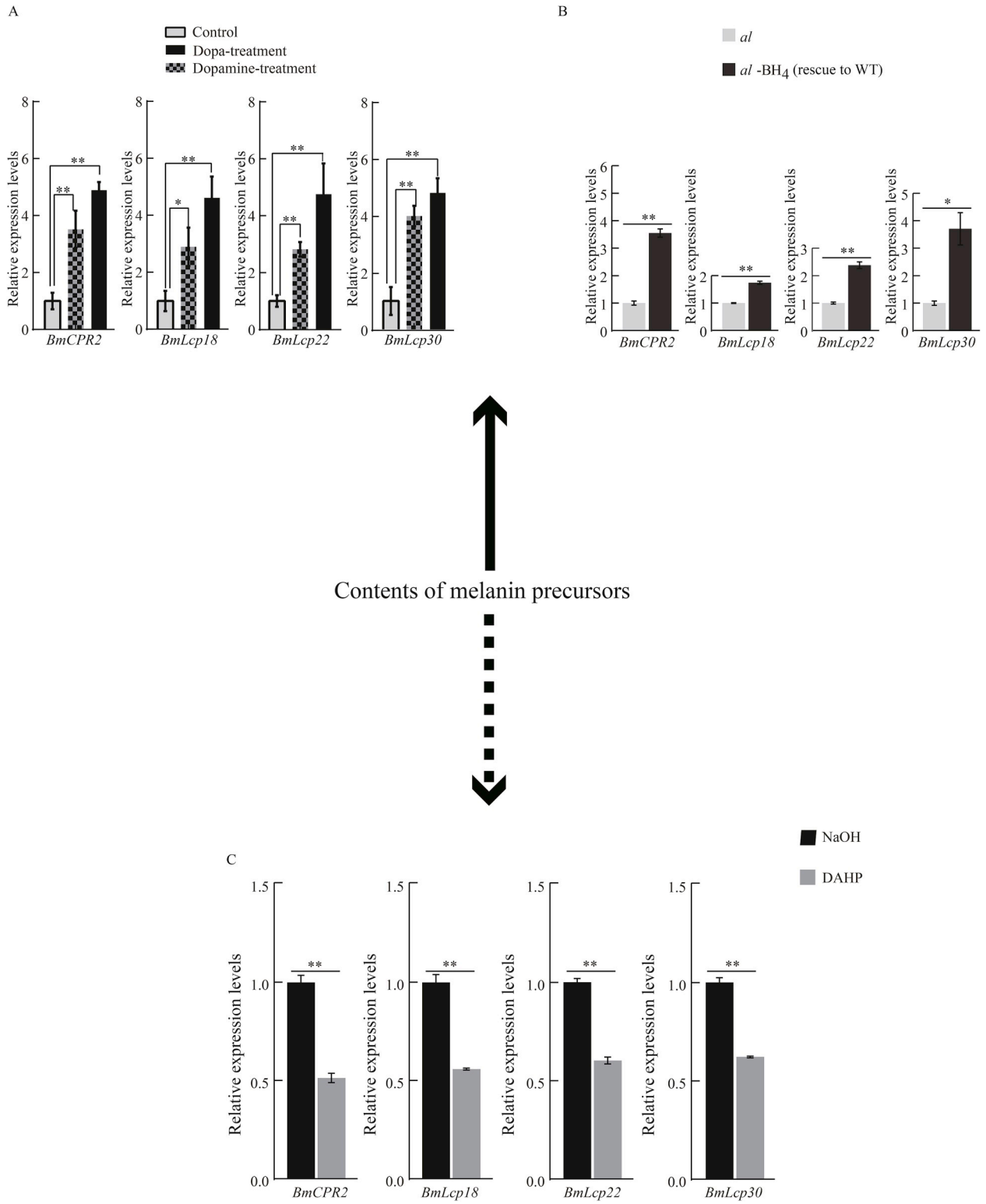

Fig. 4. Effects of melanin precursors (Fig. 6A, in *BmE* cells) and BH_4 (Fig. 6B and C, in *vivo*) on the expression of cuticular protein-encoding genes. *t*-test, n = 3, asterisks denote statistical significance, $*p < 0.05$; $**p < 0.01$.

BmLcp genes (Fig. S6).

3.4. Phenotypic observation and expression of cuticular protein-encoding genes after L-Dopa and dopamine treatment

After incubation with 5 mM melanin precursors for 24 h, the cuticles of larvae showed melanism, whereas the control group did not (Fig. 5A). Simultaneously, the expression of *BmCPR2*, *BmLcp18*, *BmLcp22*, and *BmLcp30* in the melanin precursor treatment groups was higher than that in the control group (Fig. 5B).

3.5. Complete masking of stony phenotypes by the p^B locus

We assessed the effects of modulating the melanic background on

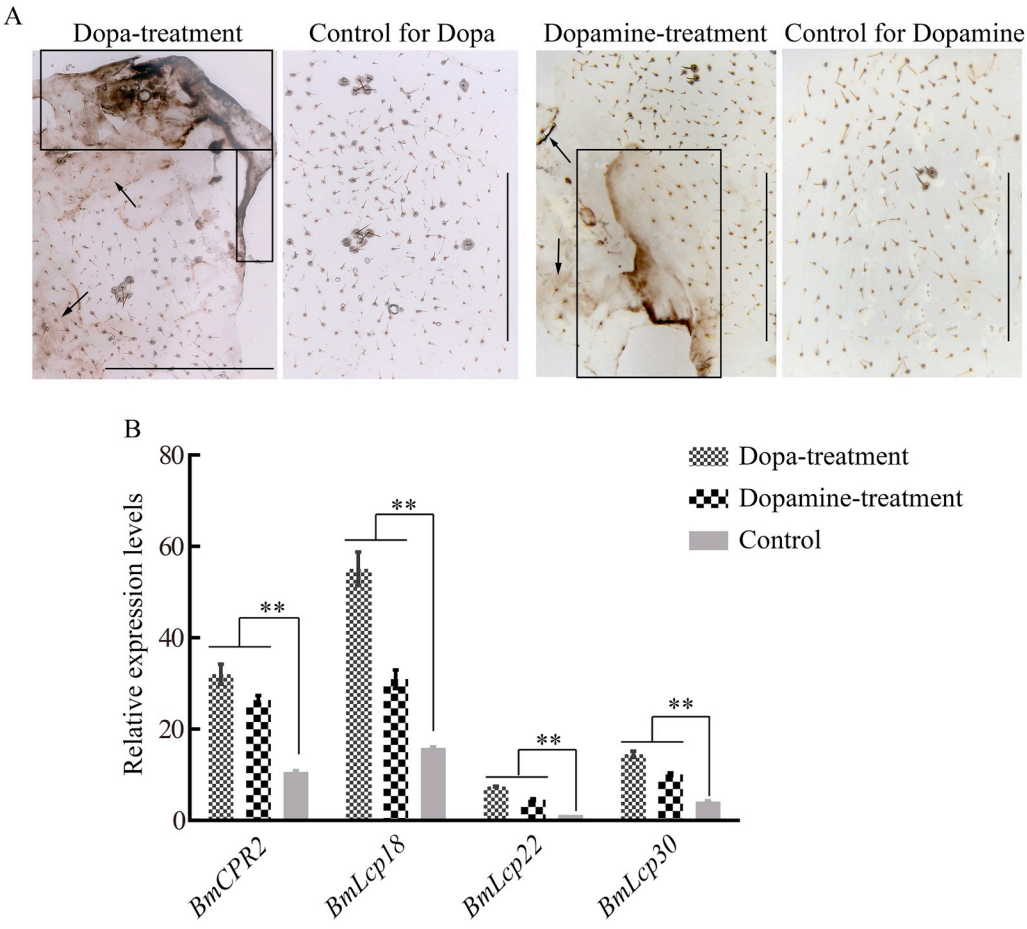

Fig. 5. Effects of treatment with melanin precursors on cuticle pigmentation and expression of cuticular protein-encoding genes. A. Cuticle pigmentation in the melanin precursor treated group and control group. Scale bar = 2 mm. The melanic regions are marked with arrows and rectangles. B. Gene expression analysis in L-Dopa and dopamine treated groups and the control group. *t*-test, n = 3, asterisks denote statistical significance, $^{**}p < 0.01$.

Table 1
Segregation patterns of the phenotypes in the progeny from the (p^B × Dazao-*stony*) × Dazao-*stony* cross.

Phenotype	Expected Ratio	Possible Genotype	Observed Number	Observed Ratio
p^B-type color pattern, normal body shape	1:4	$p^B/+^{pB}$, $+^{st}/st$	290**	2.098:4[a]
p^B-type color pattern, typical *stony*-type body shape	1:4	$p^B/+^{pB}$, st/st	0**	0:4[a]
non-melanic color pattern, normal body shape	1:4	$+^{pB}/+^{pB}$, $+^{st}/st$	138	0.998:4
non-melanic color pattern, typical *stony*-type body shape	1:4	$+^{pB}/+^{pB}$, st/st	125	0.904:4

$^{**}p < 0.01$, chi-square test ($\chi^2 = 304.8$, df = 1).
[a] Represents the actual modified Mendelian ratio.

the phenotypic defects caused by the deletion of *BmorCPR2*. After mating of the p^B and *stony* parental strains (553 BC_1 individuals), the percentage of BC_1 individuals with melanism and a normal body shape in the backcrossed population was 52% (ratio 290:553 = 2.098:4; $\chi^2 = 304.8$, df = 1, $p < 0.01$) but theoretically should have been 25% (ratio 1:4) (Table 1). No individuals with the melanic cuticle and *stony*-type body shape were found (ratio 0:553, $\chi^2 = 304.8$, df = 1, $p < 0.01$), but theoretically these individuals should have been present at 25% (ratio 1:4), equivalent to the number of individuals with melanic cuticle and normal body shape (Table 1). Genotyping results showed that approximately 25.68% (ratio 142:553 = 1.027:4) of the individuals showing a melanic color and normal body shape in the BC_1 population from the p^B × *stony* cross had the $p^B/+^{pB}$, *st/st* genotypes (Fig. 6A, Table 4). The I/IF ratio was 4, which was similar to that in $p^B/+^{pB}$, $+^{st}/st$ individuals (26.94%, ratio 149:553 = 1.070:4) and was also not significantly different from that in the wild-type individuals (Fig. 6B) (Qiao et al., 2014). Together, these results suggested that defective phenotypes were masked when the p^B locus was induced into the *stony* mutant.

3.6. No typical stony-type phenotype was observed in st/st genotyped progeny containing p^S or p^M loci

In the cross of p^S × *stony* (331 F_2 individuals), 64.3% of F_2 progeny showed a p^S-type color pattern and normal body shape (ratio 213:331 = 10.296:16; theoretical ratio, 9:16) (Table 2). We did not find individuals with a typical *stony*-type body shape and defective adaptability under the melanism background (theoretical ratio, 3:16) ($\chi^2 = 65.9$, df = 1, $p < 0.01$, see Table 2). Genotyping analysis indicated that 57.7% (ratio 191:331 = 9.233:16) of individuals with the $p^S/\_$, $+^{st}/\_$ genotype (Table 4, Fig. S7A), 6.04% (ratio 20:331 = 0.967:16) of individuals with the p^S/p^S, *st/st* genotype (Fig. 6A, Table 4), and only 0.604% (ratio 2:331 = 0.097:16) of individuals with the $p^S/+^{pS}$, *st/st* genotype had melanic color and a

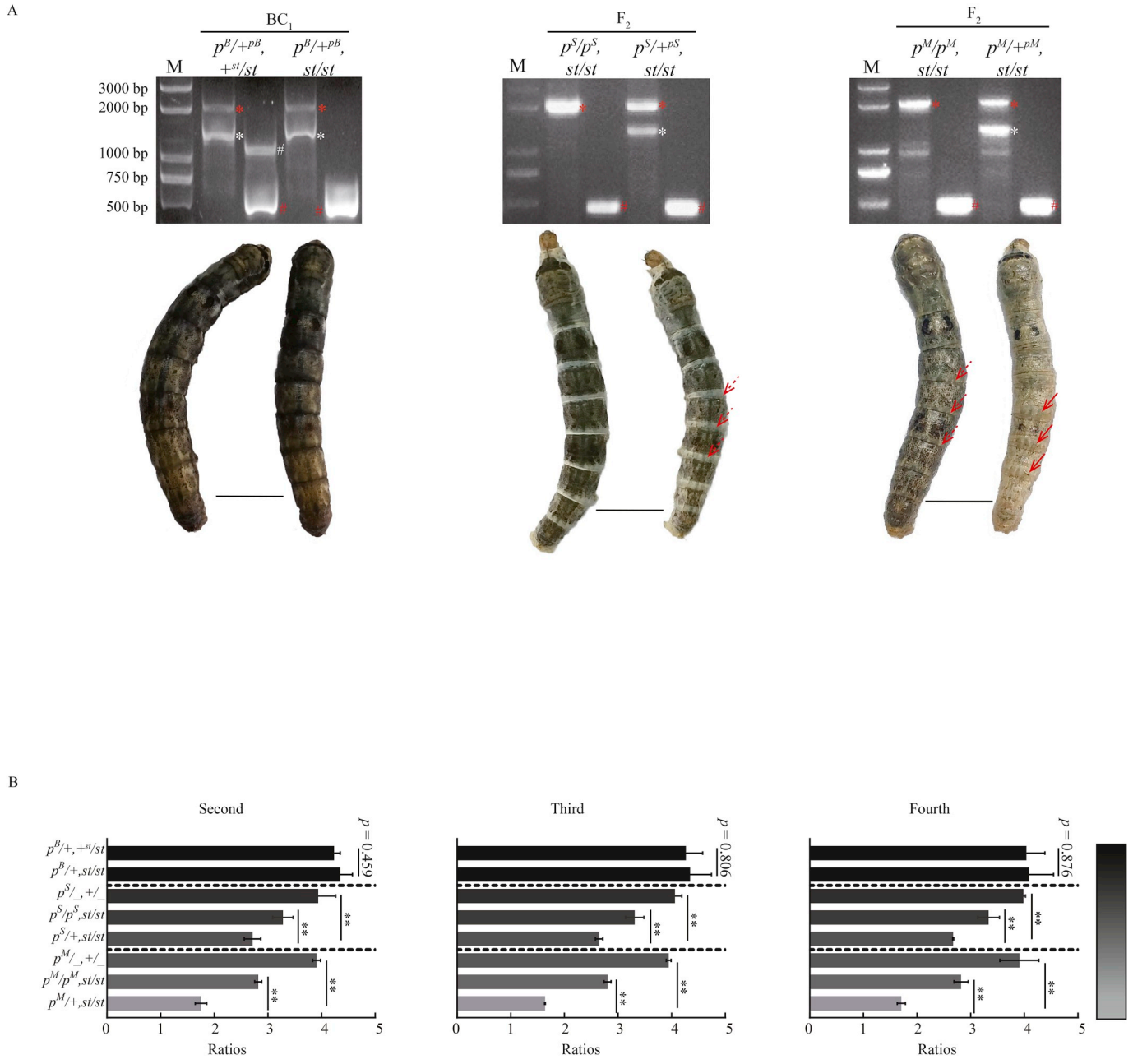

Fig. 6. Association analysis of the genotypes and phenotypes in segregated progeny from different crosses. A. Correlation analysis between the genotypes and phenotypes in self-crossed or backcrossed progeny. Scale bar is 1 cm. White and red stars represent polymorphic bands at the $+^{p}$ and melanic *p* locus (p^{M}, p^{S}, p^{B}), respectively. Red and white hash tags represent polymorphic bands at the *st* and $+^{st}$ allele, respectively. Solid and dotted red arrows indicate the relative degree of bulging (solid red arrows represent a higher degree of bulging than that represented by the dotted red arrows). B. Ratios of the lengths of internodes and intersegmental folds in the second, third, and fourth abdominal segments of individuals with different genotypes for melanic body color, in the self-crossed or backcrossed progeny. n ≥ 3, *t*-test, asterisks denote statistical significance, $^{**}p < 0.01$.

normal body shape (Table 4). In individuals genotyped as p^{S}/p^{S}, *st/st*, the I/IF ratio was 3.3 (Fig. 6B). The I/IF ratio was lower than that of $p^{S}/\_$, $+^{st}/\_$ individuals (Fig. 6B) but higher than that reported for the *stony* mutant (1.6) (Qiao et al., 2014). Despite the slightly smaller body size of the p^{S}/p^{S},*st/st* individuals, their body shape was essentially normal (Fig. 6A). However, we found that 10.88% of F_2 progeny (ratio = 1.740:16) had a lighter melanic color and smaller body size (Fig. 6A, Table 2). Their intersegment folds were slightly bulged, and the intersegment fold length was much shorter than that of the internodes (Fig. 6). Correspondingly, their phenotypes slightly resembled the morphological features of the *stony* mutant (Fig. 6, Table 2). The genotype of these individuals was $p^{S}/+^{pS}$, *st/st*, and their I/IF ratio was approximately 2.7 (Fig. 6, Table 4), a value much higher than that of the *stony* mutant.

In the p^{M} × *stony* cross (437 F_2 individuals), 62.9% of F_2 progeny exhibited a p^{M}-type color pattern, and normal body shape or some other subtle *stony* features (very slight bulges) (ratio 275:437 = 10.068:16, the theoretical ratio is 9:16) (Table 3). In these progeny, the number of $p^{M}/\_$, and $+^{st}/_$genotyped individuals was 244 (55.8% ≈ 9:16, Table 4, Fig. S7B), and the I/IF ratio was approximately 3.9 (Fig. 6B). The genotypes for individuals with subtle *stony* features (very slight bulges) were mainly p^{M}/p^{M}, *st/st* (6.63%, ratio 29:437 = 1.062:16), with a small amount of $p^{M}/+^{pM}$, *st/st* (0.458%, ratio 2:437 = 0.073:16). The I/IF ratio of p^{M}/p^{M}, *st/st* progeny was approximately 2.8, in agreement

Table 2
Segregation patterns of the phenotypes in the progeny from the p^S × Dazao-*stony* self-cross.

Phenotype	Expected Ratio	Possible Genotype	Observed Number	Observed Ratio
p^S-type color pattern, normal body shape	9:16	$p^S/\_$, $+^{st}/\_$	213**	10.296:16[a]
p^S-type color pattern, typical *stony*-type body shape	3:16	$p^S/\_$, *st/st*	0**	0:16[a]
non-melanic color pattern, normal body shape	3:16	$+^{pS}/+^{pS}$, $+^{st}/\_$	61	2.949:16
non-melanic color pattern, typical *stony*-type body shape	1:16	$+^{pS}/+^{pS}$, *st/st*	21	1.015:16
light p^S-type color pattern, ambiguous *stony*-like body shape+	0:16	$p^S/+^{pS}$, *st/st*[b]	36	1.740:16

**$p < 0.01$, chi-square test ($\chi^2 = 65.9$, df = 1), numbers of "+" symbols represent the degree of similarity of body shape to the *stony*-type body shape.
[a] Represents the actual modified Mendelian ratio. Unexpected phenotypes in the observations are underlined.
[b] Represents suspected $p^S/+^{pS}$,*st/st* genotype of individuals with a light p^S-type color pattern and an ambiguous *stony*-like body shape+.

Table 3
Segregation patterns of the phenotypes in the progeny from p^M × Dazao-*stony* self-cross.

Phenotype	Expected Ratio	Possible Genotype	Observed Number	Observed Ratio
p^M-type color pattern, normal body shape	9:16	$p^M/\_$, $+^{st}/\_$	275**	10.068:16[a]
p^M-type color pattern, typical *stony*-type body shape	3:16	$p^M/\_$, *st/st*	0**	0:16[a]
non-melanic color pattern, normal body shape	3:16	$+^{pM}/+^{pM}$, $+^{st}/\_$	84	3.076:16
non-melanic color pattern, typical *stony*-type body shape	1:16	$+^{pM}/+^{pM}$, *st/st*	27	0.989:16
very light p^M-type color pattern, ambiguous *stony*-like body shape+++	0:16	$^{pM}/+^{pM}$, *st/st*[b]	51	1.867:16[a]

**$p < 0.01$, chi-square test ($\chi^2 = 85.4$, df = 1, $p < 0.01$), numbers of "+" symbols represent the degree of similarity body shape to the *stony*-type body shape.
[a] Represents the actual modified Mendelian ratio. Unexpected observed phenotypes are underlined.
[b] Represents suspected $p^M/+^{pM}$,*st/st* genotype of individuals with a very light p^M-type color pattern and an ambiguous *stony*-like body shape+++.

with their phenotypes (Fig. 6A and B). In addition, 11.7% (ratio 51:437 = 1.86:16) of individuals in the F_2 population were much lighter but exhibited unusual morphological features (Table 3). Their intersegment folds were more bulged and had longer length proportions. Their genotypes were identified as $p^M/+^{pM}$, *st/st*, and the I/IF ratio was 1.8 (Fig. 6A and B, Table 4), a value close to that of the *stony* mutant. Their body features resembled the phenotype of the *stony* mutant (Table 3). However, individuals with the p^M-type color pattern with the typical *stony* morphologic features and defective adaptability were not present among progeny from the p^M × *stony* cross (theoretical ratio, 3:16) ($\chi^2 = 85.4$, df = 1, $p < 0.01$, see Table 3).

3.7. Cuticle slices and gene expression analysis of melanic progeny from BC_1 and F_2 crosses involving stony and p locus alleles

In BC_1 and F_2 progeny of the genotype *st/st* with melanic cuticle, we found that the epicuticle of $p^B/+^{pB}$, $+^{st}/st$, and $p^B/+^{pB}$, *st/st* individuals densely covered the melanin protrusions. The structures of their procuticles were well organized. In contrast, the procuticle structures of $+^P+^P$, *st/st* individuals were not well organized, and some damage was observed in the exocuticle. In addition, the cuticle thickness of the $p^B/+^{pB}$, $+^{st}/st$, and $p^B/+^{pB}$, *st/st* individuals was greater than that of the $+^P+^P$, *st/st* individuals (Fig. 7A–B). Although the melanin protrusions were less in p^S/p^S, *st/st* individuals than $p^B/+^{pB}$, $+^{st}/st$ and $p^B/+^{pB}$, *st/st* individuals, no disordered procuticles were observed (Fig. 7A). The cuticle thickness was slightly less than that of the $p^B/+^{pB}$, $+^{st}/st$ and $p^B/+^{pB}$, *st/st* individuals. The cuticular melanin protrusions in the $p^S/+^{pS}$, *st/st* individuals were less than those in the p^S/p^S, *st/st* individuals, and the procuticles were normally arranged. Compared with those in p^S/p^S, *st/st* individuals, the exocuticles of $p^S/+^{pS}$, *st/st* individuals were not evenly distributed (Fig. 7A). Moreover, the cuticle thickness was slightly thicker than those of $+^P+^P$, *st/st* individuals. (Fig. 7B). For the p^M/p^M, *st/st* individuals, the degree of melanism, density of melanin protrusions, and chitin fiber arrangement was all similar to those of $p^S/+^{pS}$, *st/st* individuals (Fig. 7A–B). However, in $p^M/+^{pM}$, *st/st* individuals, the density of cuticle melanization and melanin protrusions was much less than that in the previously examined melanic individuals (Fig. 7A). The exocuticle was damaged to some extent, but to a lower degree than that in $+^P+^P$, *st/st* individuals, and the cuticle thickness was close to that in the $+^P+^P$, *st/st* individuals (Fig. 7A–B).

Gene expression analysis indicated that the transcript levels of *BmCPR2* in $p^B/+^{pB}$, *st/st* individuals were lower than those in $p^B/+^{pB}$, $+^{st}/st$ individuals (owing to the effects non-sense mediated decay), whereas the expression levels of other three *BmLcps* did not differ between $p^B/+^{pB}$, $+^{st}/st$ and $p^B/+^{pB}$, *st/st* individuals (Fig. 7C). However, the darker body color and the expression of cuticular protein-encoding genes in p^S/p^S, *st/st* individuals was higher than that in $p^S/+^{pS}$, *st/st* individuals (Fig. 7C). A similar result was also obtained from the p^M/p^M, *st/st* and $p^M/+^{pM}$, *st/st* individuals (Fig. 7C). In comparison with p^M/p^M, *st/st* and $p^S/+^{pS}$, *st/st* genotyped individuals, which had similar body shape characteristics, *BmCPR2* and *BmLcp18* were expressed at higher levels in p^M/p^M, *st/st* individuals than in $p^S/+^{pS}$, *st/st* individuals. *BmLcp22* and *BmLcp30* were expressed at higher levels in $p^S/+^{pS}$, *st/st* individuals than in p^M/p^M, *st/st* individuals (Fig. 7C).

4. Discussion

In the 4th molting stage of *Bombyx mori*, the new cuticle layer forms approximately 16 h during the 4th molting period, and melanin deposition in the stripe begins 24 h during the 4th molting period (Tao-Jun-Feng et al., 2014). In *Papilio* larvae, the melanin in the stripe is also deposited at the late molting stage (Futahashi et al., 2010; Futahashi and Fujiwara). In our results, the cuticular sections showed that melanin was deposited primarily in the epicuticle region, which is involved in the melanic region of *stony* mutants and WT or other melanic mutant strains. The surface physical characteristics of the melanic cuticle regions (Fig. S3A) were similar to those previously reported (Futahashi

Table 4
Actual genotyping of the melanic progeny from BC_1 and F_2 crosses involving *stony* and *p locus* alleles.

Genotypes / Phenotypes	$p^B/+^{pB}$, $+^{st}/st$	$p^B/+^{pB}$, st/st	$p^S/\_$, $+^{st}/\_$	p^S/p^S, st/st	$p^S/+^{pS}$, st/st	$p^M/\_$, $+^{st}/\_$	p^M/p^M, st/st	$p^M/+^{pM}$, st/st
p^B-type color pattern, normal body shape	148 (148/553≈1.070:4)	142[a] (142/553≈1.027:4)	-	-	-	-	-	-
p^B-type color pattern, typical *stony*-type body shape	-	-	-	-	-	-	-	-
p^S-type color pattern, normal body shape	-	-	191 (191/331 ≈9.233/16)	20[b1] (20/331≈0.967/16)	2[b2] (0.097/16)	-	-	-
p^S-type color pattern, typical *stony*-type body shape	-	-	-	-	-	-	-	-
light p^S-type color pattern, ambiguous *stony*-like body shape+	-	-	-	-	36[b3] (36/331≈1.74/16)	-	-	-
p^M-type color pattern, normal body shape	-	-	-	-	-	244 (244/437≈8.934/16)	29[c1] (29/437≈1.062/16)	2[c2] (2/437≈0.073)
p^M-type color pattern, typical *stony*-type body shape	-	-	-	-	-	-	-	-
very light p^M-type color pattern, ambiguous *stony*-like body shape+++	-	-	-	-	-	-	-	51[c3] (51/437≈1.867/16)

[a] Indicates that the actual phenotype and expected phenotype of individuals with a $p^B/+^{pB}$, *st/st* genotype do not match, thus making the Mendelian separation ratio of the actual phenotype deviate significantly (see Table 1). The dotted arrow points to the expected phenotypic characteristics of this part of the genotype. [b1] [b2] Indicate that among the individuals with a p^S-type color pattern and a normal body shape phenotype, there were approximately 0.967/16 p^S/p^S,*st/st* individuals and 0.097/16 $p^S/+^{pS}$,*st/st* individuals that did not have the expected phenotype, thus making the Mendelian segregation ratio of the actual phenotype significantly deviate from the expected phenotype (see Table 2). The dotted arrow points to the expected phenotypic characteristics of this part of the genotype. [b3] Indicates that the defective body shape of $p^S/+^{pS}$, *st/st* individuals (1.740/16) was partially masked by a light melanic body color. The dotted arrow points to the expected phenotypic characteristics of this part of the genotype. Individual aggregation, indicated by b1, b2, and b3, is the individual $p^S/\_$, *st/st* genotype, accounting for approximately 3/16 of the F_2 population. [c1] [c2] Indicate that among the individuals with a p^M-type color pattern and a normal body shape phenotype, there were approximately 1.062/16 p^M/p^M,*st/st* individuals and 0.073/16 $p^M/+^{pM}$,*st/st* individuals that did not have the expected phenotype, thus making the Mendelian segregation ratio of the actual phenotype significantly deviate from the expected phenotype (see Table 3). The dotted arrow points to the expected phenotypic characteristics of this part of the genotype. [c3] Indicates that the defective body shape of $p^M/+^{pM}$, *st/st* genotyped individuals (1.867/16) was slightly masked by a very light melanic body color. Individual aggregation, indicated by c1, c2, and c3, is the individual $p^M/\_$, *st/st* genotype, accounting for approximately 3/16 of the F_2 population.

et al., 2012; He et al., 2016; Jan et al., 2017; Tan et al., 2016). Variations in chitin content (Fig. S3B) have also been shown to be associated with cuticle melanism and expression patterns of cuticular protein-encoding genes (Balabanidou et al., 2019; Moussian et al., 2005, 2006). Deposition of melanin was accompanied by thickening of the procuticle, which contained large amounts of chitin (Figs. 1 and 5A). Regardless of the genotypes of the melanic mutants or the melanic markings in the non-melanic strains, excessive accumulation of melanin in the cuticle was tightly associated with particular cuticular physical characteristics. We speculate that this phenomenon may be beneficial in maintaining the physiological function of the melanic cuticle. The significant differences in cuticular physical features between melanic and non-melanic integument regions provide clear evidence of the effects of melanism on cuticle characteristics.

Excessive accumulation of melanin was tightly associated with significantly up-regulated expression of melanin synthase genes (Fig. S8). The up-regulation of these four genes encoding larval cuticular proteins in melanic integuments was independent of genetic background (Figs. 2 and 3, Fig. S4) (Futahashi et al., 2012; He et al., 2016; Jan et al., 2017; Wu et al., 2016). For other cuticular protein-encoding

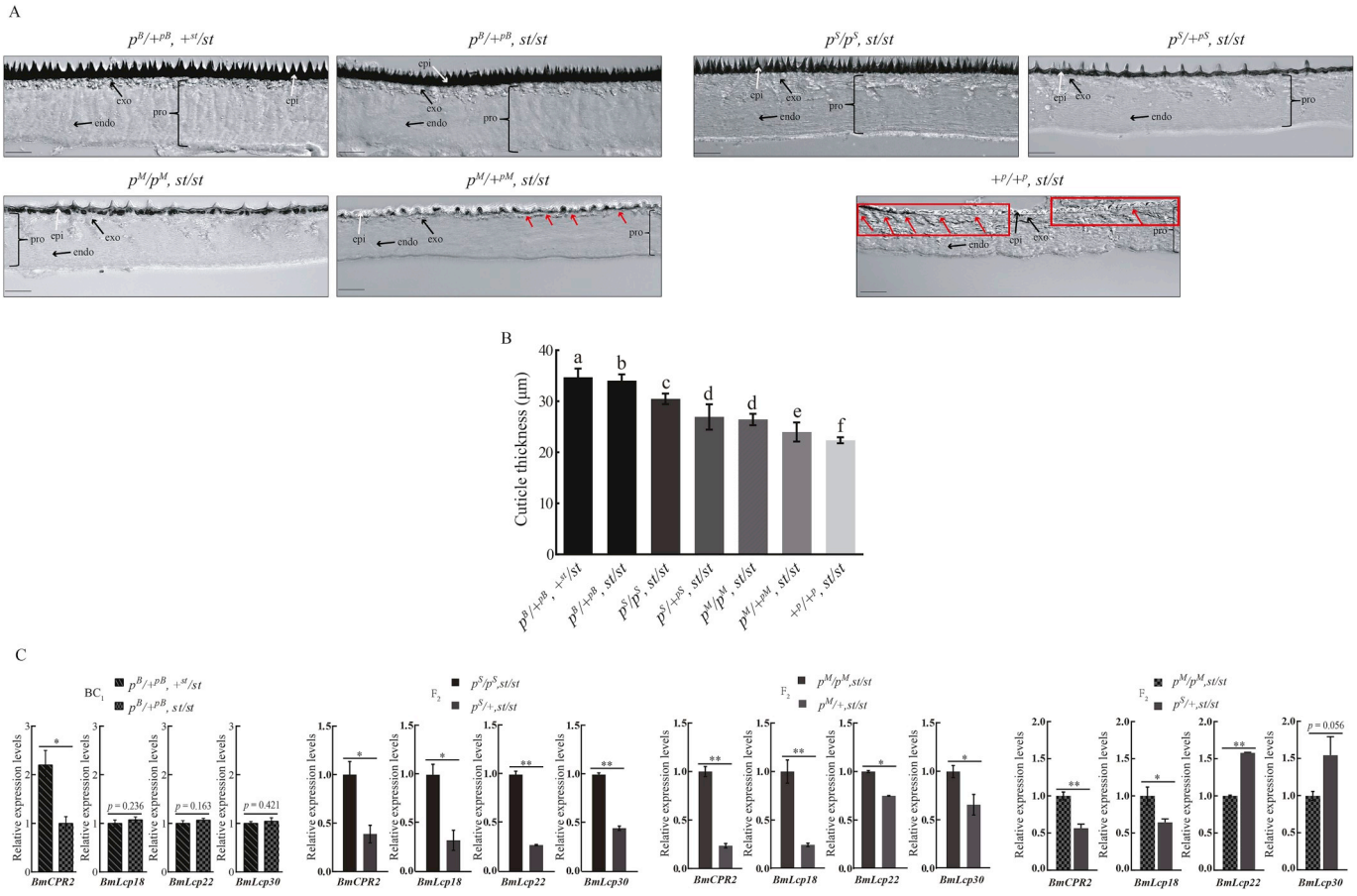

Fig. 7. Features of the cuticle cross-section and gene expression patterns in *st/st* individuals (progeny of BC_1 and F_2) under different melanic backgrounds. A. Features of the cuticle cross-section in BC_1 and F_2 progeny with different degrees of melanism. Scale bar = 10 μm. Epi: epicuticle, exo: exocuticle, endo: endocuticle, pro: procuticle. The disordered arrangement in the procuticle is boxed in red. Red arrow represents damage to the exocuticle. B. Cuticle thicknesses for all genotypes listed in Figure A. One-way ANOVA test, n = 3, F = 95.80, n = 3, $p < 0.05$. C. Expression analysis of cuticular protein-encoding genes in heterozygotic individuals at the *p* locus from back-crossed progeny of $p^B \times$ *stony* and expression analysis of cuticular protein-encoding genes in homozygotic and heterozygotic individuals at the *p* locus from self-crossed progeny of $p^S \times$ *stony*, and $p^M \times$ *stony*, only if the cuticle was melanic and the genotype was homozygous recessive at the *stony* locus. *t*-test, n = 3, asterisks denote statistical significance, *$p < 0.05$; **$p \leq 0.01$. (For interpretation of the references to color in this figure legend, the reader is referred to the Web version of this article.)

genes, even some predominantly expressed in non-larval stages (Such as *BmCPG13* and *BmCPR68*) (Xia et al., 2007), their expression was still up-regulated in the melanic integument regions (Fig. S8). These results suggested that this correlation is universal. In contrast, the up-regulation of cuticular protein-encoding genes did not affect cuticle melanism (Tajiri, 2017; Xiong et al., 2017). The degree of melanism in stripes in the *stony* mutant was less than that in the WT (Fig. S9). The comparison of stripes between $p^S/+^{pS}$, $+^{st}/+^{st}$ and $p^S/+^{pS}$, *st/st* individuals also showed similar results (Figs. 3A and 6A). Thus, we speculate that *BmCPR2* is also involved in maintaining the cuticular coloring pattern. Previous studies have also reported the importance of larval cuticular protein-encoding genes in maintaining the melanic body color of larvae (Xiong et al., 2017). Additionally, structural characteristics of different cuticular layers are not produced independently: mutations affecting one protein located in a certain cuticular layer also affect the structures of other cuticular layers (Mun et al., 2019; Sobala and Adler, 2016). Therefore, we considered that during cuticle development, when the melanism-promoting signals occur, the up-regulation of *BmCPR2*, *BmLcp18*, *BmLcp22*, and *BmLcp30* may be a necessary adaptation enabling the dynamic process of excess melanin deposition, and the maintenance and stability of the structural characteristics and physical properties of melanic cuticles. In further research, detecting the dynamic changes in melanin deposition and the distribution of cuticular proteins in detail would contribute to exploration of the interactions among major cuticle components.

The variations in expression of certain cuticular protein-encoding genes did not affect other members (Fig. S5 and S6), in agreement with findings in other reports (Arakane et al., 2012; Noh et al., 2015; Xiong et al., 2017). These results indicate that there is no direct regulation of expression between larval cuticular protein-encoding genes with similar expression and function. Moreover, to our knowledge, there is no evidence suggesting that cuticular proteins can enter the nucleus and regulate gene expression by acting as transcription factors. Extensive accumulation of melanin precursors in epidermal cells is essential for cuticle melanization; thus, melanism promotes the expression of cuticular protein-encoding genes, a process driven by coordination between the accumulation of melanin precursors and the expression of cuticular protein-encoding genes. Our results demonstrated that changes in intracellular melanin precursors are important for regulating the expression of cuticular protein-encoding genes (Figs. 4 and 5). Some evidence also supports that melanin precursors can regulate gene expression through the receptors of melanin precursors (Berke et al., 1998; Konradi et al., 1996; Westin et al., 2001). Furthermore, BH_4 and DAHP affect the synthesis of melanin precursors, thus leading to coordinated variations in the expression of cuticular proteins; however, these two chemicals do not directly impair the extracellular accumulation of melanin or protein-protein interactions in the cuticle. More importantly, treatment introducing melanin precursor into non-melanic

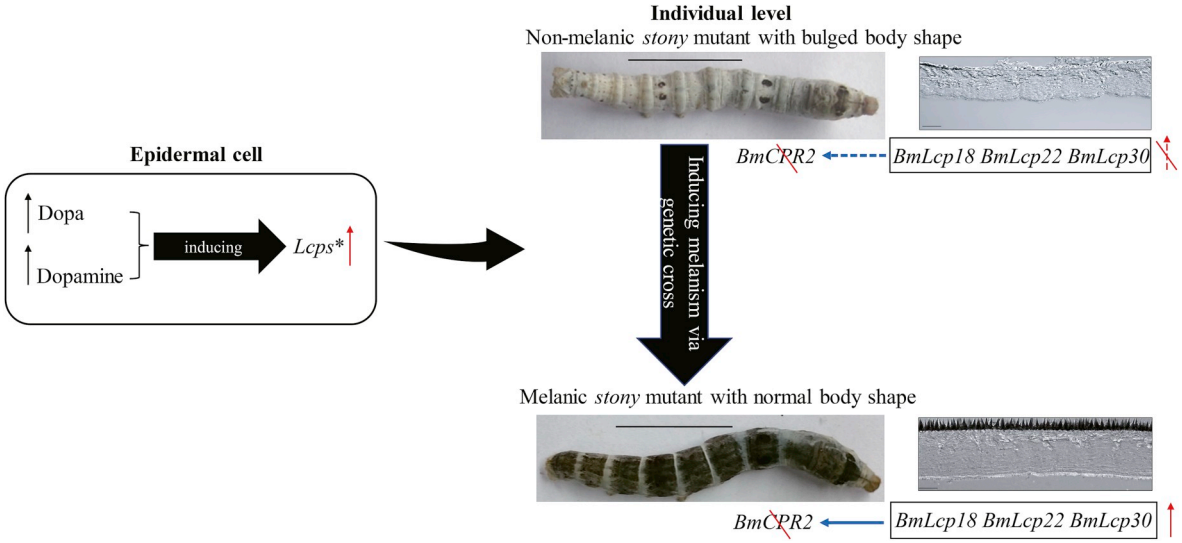

Fig. 8. Schematic overview of the effects of melanin precursors on the expression of cuticular protein-encoding genes as well as larval body shape. Scale bar = 1 cm. In epidermal cells, vertical black arrows indicate the increase in melanin precursor content, and the red arrow indicates increased expression of larval cuticular protein-encoding genes (*Lcps*). Asterisks represent similar expression patterns and functions of the *Lcps*. At the individual level, the red backslash indicates partial deletion of the *BmCPR2* CDS sequence and BmCPR2 dysfunction. Genes with similar expression patterns and functions to those of *BmCPR2* are boxed; the red dotted arrow with red backslash indicates that the expression of larval cuticular protein-encoding genes in the box was not up-regulated. The blue dotted arrow indicates that the boxed genes could not compensate for the deficiency caused by the function loss of BmCPR2. The red solid arrow indicates that the boxed genes were up-regulated under a melanism background. The blue solid arrow indicates that the boxed genes were able to compensate for the deficiency caused by the loss of BmCPR2 function.

integuments results in a melanic cuticular phenotype and up-regulated expression of four larval cuticular protein-encoding genes (Fig. 5); these results establish a direct relationship between melanin precursors and larval cuticular protein-encoding genes. We believe that up-regulation of *BmCPR2*, *BmLcp18*, *BmLcp22*, and *BmLcp30* may have occurred simultaneously, owing to excessive amounts of melanin precursors, but these four RR1-type *BmLcps* are not expected to be mutually regulated. Notably, several studies have found that mutations in genes affecting melanin synthesis or regulation influence not only the pigmentation but also the morphology and structure of the cuticle (Concha et al., 2019; Massey et al., 2019; Matsuoka and Monteiro, 2017; Mun et al., 2019). These genes are directly or indirectly involved in the synthesis and accumulation of melanin precursors. From the perspective of the effects on cuticle characteristics, variations in melanin precursor content should be closely associated with changes in cuticular structure. Thus, we suggest that the regulation of cuticular protein-genes by melanin precursors may lie at the core of this association. Further analyses will be performed to explore the response elements in the regulatory sequences of *BmLcp* genes and to determine the detailed molecular mechanisms of melanin precursors.

Although there are 148 RR-type cuticular proteins in the silkworm genome (Futahashi et al., 2008), RR1-type *BmLcp* genes were chosen on the basis of their similar expression patterns (Fig. S1) and chitin-binding characteristics during larval development (Dong et al., 2016; Liang et al., 2010; Nakato et al., 1994, 1997; Okamoto et al., 2008; Qiao et al., 2014; Tang et al., 2010; Xiong et al., 2017). Additionally, the near isogenic line Dazao-*stony* was almost genetically and phenotypically identical to the wild-type Dazao strain with *BmCPR2* knockout (Qiao et al., 2014). We cannot exclude the possibility that other cuticular protein-encoding genes (up-regulated under melanic cuticle regions) might participate in maintaining the structure of the melanic cuticle. We focused on these four RR1-type *BmLcps* as typical representatives, to enable specific analysis of the compensatory effects and the relevant phenotypic cuticular characteristics under the larval developmental stages and conditions. In follow-up research, we will introduce a melanism background into lines with knockout of the other three cuticular protein-encoding genes (*BmLcp18*, *BmLcp22*, and *BmLcp30*) to verify the complementarity effect hypothesis.

Because homozygous p^B mutations are lethal (Banno et al., 2005; Xiang, 1995), we were unable to obtain F_2 progeny with the p^B/p^B, *st/st* genotype. However, individuals with the $p^B/+^{pB}$, $+^{st}/st$ and $p^B/+^{pB}$, *st/st* genotypes had almost the same body shape and degree of melanism (Fig. 6A). In the back-cross progeny of $p^B \times$ *stony*, the observed number of individuals with p^B-type melanism and normal body shape was twice that expected (Fig. 6A and B, Table 1, Table 4). Among these individuals, 25% of $p^B/+^{pB}$, *st/st* individuals were suspected to have p^B-type melanic cuticles and a *stony*-type body shape, but this phenotype was not observed (Fig. 6A and B, Table 1, Table 4). This result may be explained by the epistatic effect of excessive melanism on the *stony*-type body shape phenotype. Similarly, in the progeny of $p^S \times$ *stony*, an additional 1/16 of individuals had a p^S-type color pattern and normal body shape, a proportion greater than expected (theoretical ratio, 9:16); moreover, approximately 1/16 of individuals had the p^S/p^S, *st/st* genotype (theoretically, they should have had a p^S-type color pattern with a typical *stony*-type body shape) (Fig. 6A and B, Table 2, Table 4). In addition, 1.740/16 of $p^S/+^{pS}$, *st/st* individuals (close to 2/16) with light melanic color were practically masked cuticular defects, and therefore most of them exhibited the ambiguous *stony*-like body shape (approximately 0.097/16 individuals with the genotype $p^S/+p^S$, *st/st* had normal body shape and therefore were not included in the calculation) (Fig. 6A and B, Table 2, Table 4). The sum of the proportions of p^S/p^S, *st/st* individuals to $p^S/+^{pS}$, *st/st* individuals (2.804/16) was very close to the expected value of 3/16 for $p^S/\_$, *st/st* individuals (Table 2, Table 4). Moreover, the ratio deviation of the genotype and phenotype of $p^M \times$ *stony* progeny was similar to that of $p^S \times$ *stony* progeny (Fig. 6A and B, Table 3, Table 4). The proportion of $p^B/+^{pB}$, *st/st* (ratio = 1.027:4), *ps*/$+^{pS}$, *st/st* (ratio = 1.837:16), and $p^M/+^{pM}$, *st/st* (ratio = 1.940:16) genotyped individuals was close to the expected value (1:4, 2:16, and 2:16, respectively) (Tables 1–4). The different degrees of melanism with a homozygous or heterozygous *p* locus led to different levels of epistatic effects (Figs. 6 and 7, Tables 1–4). These phenotypes were completely or partially masked by melanism (Fig. 6; Tables 1–4). These characteristics further validate the masking effect of melanism on defective body shape at the molecular level. Considering

the phenotypic characteristics, cuticular section structure, and expression of cuticular protein-encoding genes in the progeny with melanic color and the *st/st* genotype, we suggest that the epistatic effect may be due to up-regulation of cuticular protein-encoding genes under a melanism background, thereby resulting in accumulation of more cuticular proteins with similar functions in the cuticle and masking the cuticular defects in *st/st* individuals. The degree of compensation was in the order $p^B/+^{pB}$, *st/st* > p^S/p^S, *st/st* > (p^M/p^M, *st/st* or $p^S/+^{pS}$, *st/st*) > $p^M/+^{pM}$, *st/st*, which corresponds well to the gradual decrease in the degree of melanism (Figs. 6 and 7, Tables 1–4). The compensatory effects of melanic body color on defective cuticular features also provided new evidence explaining how melanism can be a beneficial trait (Liu et al., 2015b; Mallet and Hoekstra, 2016; True, 2003; Wilson et al., 2001; Wittkopp and Beldade, 2009; Wittkopp et al., 2003).

On the basis of our results, we propose the following model to explain our findings: 1) the larval cuticular protein-encoding genes *BmCPR2*, *BmLcp18*, *BmLcp22*, and *BmLcp30* are up-regulated by the induction of accumulated melanin precursors, and their expression levels are positively correlated with the degree of melanism; this induction pattern ensures the formation of normal structural features of the melanic cuticle; 2) if a melanism background is introduced into *BmCPR2* deleted individuals through a genetic cross, other cuticular protein genes with similar functions, *BmLcp18*, *BmLcp22*, and *BmLcp30* (induced by melanin precursors), can compensate for the morphological and adaptive defects caused by dysfunctional *BmCPR2*; the degree of compensation increases with the accumulation of melanin (Fig. 8). Because excess melanin and cuticular proteins commonly occur together in other insects (Andersen, 2010; Cohen and Moussian, 2016; Moussian, 2010), and homologues of the four RR1-type BmLcps are widely distributed in Lepidoptera (Table S2), we presume that the induction phenomenon, as well as its corresponding biological importance might be conserved in Lepidoptera.

Author contribution

LQ and FYD conceived and coordinated the study and wrote the paper. LQ and FYD designed the experiments. LQ, ZWY, RXW, GX, HH, SZH, and JBS performed the experiments. LQ, GX, YJH, and XLT analyzed the data. LQ, JM, LRC, BC, and CL revised the paper. All authors read and approved the final manuscript.

Declaration of competing interests

The authors declare no competing financial interests.

Acknowledgments

We thank Dr. Wei Sun, Dr. Tianzhu Xiong, Dr. Minjin Han, Dr. Chunlin Li, Dr. Yonggang Hu, Dr. Kunpeng Lu, and Dr. Yaqun Xin for providing valuable advice. This work was supported by the National Natural Science Foundation of China (Nos. 31830094, 31772527), the Hi-Tech Research and Development 863 Program of China (grant No. 2013AA102507), the Natural Science Foundation Project of ChongQing (CSTC) (No. cstc2017jcyjAX0023), the Open Foundation of The State Key Laboratory of Silkworm Genome Biology (SKLSGB1819-6), the Bayu young scholars program (BYQNCS2019009), the Scientific and Technological Research Program of the Chongqing Municipal Education Commission (KJQN201900523), and the Funds of China Agricultural Research System (No. CARS-18-ZJ0102).

Appendix A. Supplementary data

Supplementary data to this article can be found online at https://doi.org/10.1016/j.ibmb.2020.103315.

References

Andersen, S.O., 2010. Insect cuticular sclerotization: a review. Insect Biochem. Mol. Biol. 40, 166–178.
Arakane, Y., Lomakin, J., Gehrke, S.H., Hiromasa, Y., Tomich, J.M., Muthukrishnan, S., Beeman, R.W., Kramer, K.J., Kanost, M.R., 2012. Formation of rigid, non-flight forewings (elytra) of a beetle requires two major cuticular proteins. PLoS Genet. 8, e1002682.
Balabanidou, V., Kefi, M., Aivaliotis, M., Koidou, V., Girotti, J.R., Mijailovsky, S.J., Juárez, M.P., Papadogiorgaki, E., Chalepakis, G., Kampouraki, A., Nikolaou, C., Ranson, H., Vontas, J., 2019. Mosquitoes cloak their legs to resist insecticides. Proc. R. Soc. Biol. Sci. 286, 20191091.
Banno, Y., Fujii, H., Kawaguchi, Y., Yamamoto, K., Nishikawa, K., Nishisaka, A., Tamura, K., Eguchi, S., 2005. A Guide to the Silkworm Mutants: 2005 Gene Name and Gene Symbol. Kyusyu University, Fukuoka, Japan.
Berke, J.D., Paletzki, R.F., Aronson, G.J., Hyman, S.E., Gerfen, C.R., 1998. A complex program of striatal gene expression induced by dopaminergic stimulation. J. Neurosci. 18, 5301–5310.
Chaudhari, S.S., Arakane, Y., Specht, C.A., Moussian, B., Boyle, D.L., Park, Y., Kramer, K.J., Beeman, R.W., Muthukrishnan, S., 2011. Knickkopf protein protects and organizes chitin in the newly synthesized insect exoskeleton. Proc. Natl. Acad. Sci. USA 108, 17028–17033.
Cohen, E., Moussian, B., 2016. Extracellular Composite Matrices in Arthropods. Springer, Switzerland.
Concha, C., Wallbank, R.W.R., Hanly, J.J., Fenner, J., Livraghi, L., Rivera, E.S., Paulo, D.F., Arias, C., Vargas, M., Sanjeev, M., Morrison, C., Tian, D., Aguirre, P., Ferrara, S., Foley, J., Pardo-Diaz, C., Salazar, C., Linares, M., Massardo, D., Counterman, B.A., Scott, M.J., Jiggins, C.D., Papa, R., Martin, A., McMillan, W.O., 2019. Interplay between developmental flexibility and determinism in the evolution of mimetic < em > Heliconius < /em > wing patterns. Curr. Biol. 29, 3996–4009 e3994.
Dai, F., Lu, C., Xiang, Z., 2000. A study on the genetics of “new stony”-a natural mutant in silkworm. Acta Sericol. Sin. 26, 53–55.
Delgado-Esteban, M., Almeida, A., Medina, J.M., 2002. Tetrahydrobiopterin deficiency increases neuronal vulnerability to hypoxia. J. Neurochem. 82, 1148–1159.
Dong, Z., Zhang, W., Zhang, Y., Zhang, X., Zhao, P., Xia, Q., 2016. Identification and characterization of novel chitin-binding proteins from the larval cuticle of silkworm, Bombyx mori. J. Proteome Res. 15, 1435–1445.
Fujii, T., Abe, H., Kawamoto, M., Katsuma, S., Banno, Y., Shimada, T., 2013. Albino (al) is a tetrahydrobiopterin (BH_4)-deficient mutant of the silkworm *Bombyx mori*. Insect Biochem. Mol. Biol. 43, 594-600.
Futahashi, R., Banno, Y., Fujiwara, H., 2010. Caterpillar color patterns are determined by a two-phase melanin gene prepatterning process: new evidence from tan and lac-case2. Evol. Dev. 12.
Futahashi, R., Fujiwara, H., Melanin-synthesis enzymes coregulate stage-specific larval cuticular markings in the swallowtail butterfly,Papilio Xuthus. 215, 519-529.
Futahashi, R., Fujiwara, H., 2005. Melanin-synthesis enzymes coregulate stage-specific larval cuticular markings in the swallowtail butterfly, *Papilio xuthus*. Dev. Gene. Evol. 215, 519–529.
Futahashi, R., Fujiwara, H., 2006. Expression of one isoform of GTP cyclohydrolase I coincides with the larval black markings of the swallowtail butterfly, Papilio xuthus. Insect Biochem. Mol. Biol. 36, 63–70.
Futahashi, R., Okamoto, S., Kawasaki, H., Zhong, Y.S., Iwanaga, M., Mita, K., Fujiwara, H., 2008. Genome-wide identification of cuticular protein genes in the silkworm, Bombyx mori. Insect Biochem. Mol. Biol. 38, 1138–1146.
Futahashi, R., Shirataki, H., Narita, T., Mita, K., Fujiwara, H., 2012. Comprehensive microarray-based analysis for stage-specific larval camouflage pattern-associated genes in the swallowtail butterfly, *Papilio xuthus*. BMC Biol. 10, 46.
Guan, X., Middlebrooks, B.W., Alexander, S., Wasserman, S.A., 2006. Mutation of TweedleD, a member of an unconventional cuticle protein family, alters body shape in *Drosophila*. Proc. Natl. Acad. Sci. USA 103, 16794–16799.
He, S.Z., Tong, X.L., Lu, K.P., Lu, Y.R., Luo, J.W., Yang, W.H., Chen, M., Han, M.J., Hu, H., Lu, C., Dai, F.Y., 2016. Comparative analysis of transcriptomes among *Bombyx mori* strains and sexes reveals the genes regulating melanic morph and the related phenotypes. PLoS One 11.
Hopkins, T.L., Kramer, K.J., 1992. Insect cuticle sclerotization. Annu. Rev. Entomol. 37, 273–302.
Hu, F., Zhang, G.N., Wang, J.J., 2009. Scanning electron microscopy studies of antennal sensilla of bruchid beetles, Callosobruchus chinensis (L.) and Callosobruchus maculatus (F.) (Coleoptera: bruchidae). Micron 40, 320–326.
Hu, Y.G., Shen, Y.H., Zhang, Z., Shi, G.Q., 2013. Melanin and urate act to prevent ultraviolet damage in the integument of the silkworm, Bombyx mori. Arch. Insect Biochem. Physiol. 83, 41–55.
Jan, S., Li, C., Liu, S., Liu, X., Zhu, F., Hafeez, M., Wang, M., 2017. Microscopic cuticle structure comparison of pupal melanic and wild strain of Spodoptera exigua and their gene expression profiles in three time points. Microb. Pathog. 114, 483–493.
Kanekatsu, R., Banno, Y., Nagashima, E., Miyashita, T., 1988. Genetical studies on a new spontaneous mutant “Bamboo” (*Bo*) of the silkworm. J. Seric. Sci. Jpn. 57, 151–156.
Konradi, C., Leveque, J.C., Hyman, S.E., 1996. Amphetamine and dopamine-induced immediate early gene expression in striatal neurons depends on postsynaptic NMDA receptors and calcium. J. Neurosci. 16, 4231–4239.
Liang, J., Zhang, L., Xiang, Z., He, N., 2010. Expression profile of cuticular genes of silkworm, *Bombyx mori*. BMC Genomics 11, 173.
Liu, S., Wang, M., Li, X., 2015a. Pupal melanization is associated with higher fitness in Spodoptera exigua. Sci. Rep. 5.

Liu, S.S., Wang, M., Li, X.C., 2015b. Pupal melanization is associated with higher fitness in *Spodoptera exigua*. Sci. Rep. UK 5.
Mallet, J., Hoekstra, H.E., 2016. Ecological genetics: a key gene for mimicry and melanism. Curr. Biol. 26, R802–R804.
Massey, J.H., Chung, D., Siwanowicz, I., Stern, D.L., Wittkopp, P.J., 2019. The yellow gene influences Drosophila male mating success through sex comb melanization. eLife 8, e49388.
Matsuoka, Y., Monteiro, A., 2017. Melanin pathway genes regulate color and morphology of butterfly wing scales. Mech. Dev. 24 (1), 56–65.
Min, C., Song, J.B., Zhi-Quan, L.I., Tang, D.M., Tong, X.L., Dai, F.Y., 2016. Progress and perspective of silkworm as a model of human diseases for drug screening. Acta Pharm. Sin. 51 (5), 690–697.
Mitchell, B.M., Dorrance, A.M., Webb, R.C., 2003. GTP cyclohydrolase 1 inhibition attenuates vasodilation and increases blood pressure in rats. Am. J. Physiol. Heart Circ. Physiol. 285, H2165–H2170.
Moussian, B., 2010. Recent advances in understanding mechanisms of insect cuticle differentiation. Insect Biochem. Mol. Biol. 40, 363–375.
Moussian, B., Schwarz, H., Bartoszewski, S., Nusslein-Volhard, C., 2005. Involvement of chitin in exoskeleton morphogenesis in *Drosophila melanogaster*. J. Morphol. 264, 117–130.
Moussian, B., Tang, E., Tonning, A., Helms, S., Schwarz, H., Nusslein-Volhard, C., Uv, A.E., 2006. Drosophila Knickkopf and Retroactive are needed for epithelial tube growth and cuticle differentiation through their specific requirement for chitin filament organization. Development 133, 163–171.
Mun, S., Noh, M.Y., Kramer, K.J., Muthukrishnan, S., Arakane, Y., 2019. Gene functions in adult cuticle pigmentation of the yellow mealworm, Tenebrio molitor. Insect Biochem. Mol. 103291.
Nakato, H., Shofuda, K., Izumi, S., Tomino, S., 1994. Structure and developmental expression of a larval cuticle protein gene of the silkworm, Bombyx mori. Biochim. Biophys. Acta 1218, 64–74.
Nakato, H., Takekoshi, M., Togawa, T., Izumi, S., Tomino, S., 1997. Purification and cDNA cloning of evolutionally conserved larval cuticle proteins of the silkworm, Bombyx mori. Insect Biochem. Mol. Biol. 27, 701–709.
Noh, M.Y., Muthukrishnan, S., Kramer, K.J., Arakane, Y., 2015. *Tribolium castaneum* RR-1 cuticular protein TcCPR4 is required for formation of pore canals in rigid cuticle. PLoS Genet. 11.
Noh, M.Y., Muthukrishnan, S., Kramer, K.J., Arakane, Y., 2016. Cuticle formation and pigmentation in beetles. Curr. Opin. Insect Sci. 17, 1–9.
Okamoto, S., Futahashi, R., Kojima, T., Mita, K., Fujiwara, H., 2008. Catalogue of epidermal genes: genes expressed in the epidermis during larval molt of the silkworm *Bombyx mori*. BMC Genomics 9, 396.
Oota, K., Kanekatsu, R., 1993. Morphological studies on the Bamboo (*Bo*) mutant of the silkworm, *Bombyx mori*. J. Seric. Sci. Jpn. 62, 448–454.
Qiao, L., Xiong, G., Wang, R.X., He, S.Z., Chen, J., Tong, X.L., Hu, H., Li, C.L., Gai, T.T., Xin, Y.Q., Liu, X.F., Chen, B., Xiang, Z.H., Lu, C., Dai, F.Y., 2014. Mutation of a cuticular protein, BmorCPR2, alters larval body shape and adaptability in silkworm. Bombyx Mori. Genet. 196, 1103–1115.
Shofuda, K., Togawa, T., Nakato, H., Tomino, S., Izumi, S., 1999. Molecular cloning and characterization of a cDNA encoding a larval cuticle protein of Bombyx mori. Comp. Biochem. Physiol. B Biochem. Mol. Biol. 122, 105–109.
Sobala, L.F., Adler, P.N., 2016. The gene expression program for the formation of wing cuticle in Drosophila. PLoS Genet. 12, e1006100.
Suderman, R.J., Dittmer, N.T., Kanost, M.R., Kramer, K.J., 2006. Model reactions for insect cuticle sclerotization: cross-linking of recombinant cuticular proteins upon their laccase-catalyzed oxidative conjugation with catechols. Insect Biochem. Mol. Biol. 36, 610–611.
Tajiri, R., 2017. Cuticle itself as a central and dynamic player in shaping cuticle. Curr. Opin. Insect Sci. 19, 30–35.
Tan, D., Tong, X.L., Hu, H., Wu, S.Y., Li, C.L., Xiong, G., Xiang, Z.H., Dai, F.Y., Lu, C., 2016. Morphological characterization and molecular mapping of an irradiation-induced Speckled mutant in the silkworm, *Bombyx mori*. Insect Mol. Biol. 25, 93–104.
Tang, L., Liang, J., Zhan, Z., Xiang, Z., He, N., 2010. Identification of the chitin-binding proteins from the larval proteins of silkworm, Bombyx mori. Insect Biochem. Mol. Biol. 40, 228–234.
Tao-Jun-Feng, S.U., Xia, C.L., Yan-Jun, L.I., Zhang, X.Y., Zhou, M.T., Zhang, Y.X., Liu, C., Xia, Q.Y., 2014. Anatomical observation of melanin formation in markings on integuments of Bombyx mori. Sci. Seric. (Q.) 40 (3), 445–451.
Tong, X., Liang, P., Wu, S., Li, Y., Qiao, L., Hu, H., Xiang, Z., Lu, C., Dai, F., 2018. Disruption of PTPS gene causing pale body color and lethal phenotype in the silkworm, Bombyx mori. Int. J. Mol. Sci. 19.
True, J.R., 2003. Insect melanism: the molecules matter. Trends Ecol. Evol. 18, 640–647.
Van Belleghem, S.M., Rastas, P., Papanicolaou, A., Martin, S.H., Arias, C.F., Supple, M.A., Hanly, J.J., Mallet, J., Lewis, J.J., Hines, H.M., Ruiz, M., Salazar, C., Linares, M., Moreira, G.R.P., Jiggins, C.D., Counterman, B.A., McMillan, W.O., Papa, R., 2017. Complex modular architecture around a simple toolkit of wing pattern genes. Nat. Ecol. Evol. 1.
Westin, J.E., Andersson, M., Lundblad, M., Cenci, M.A., 2001. Persistent changes in striatal gene expression induced by long-term L-DOPA treatment in a rat model of Parkinson's disease. Eur. J. Neurosci. 14, 1171–1176.
Wilson, K., Cotter, S.C., Reeson, A.F., Pell, J.K., 2001. Melanism and disease resistance in insects. Ecol. Lett. 4, 637–649.
Wittkopp, P.J., Beldade, P., 2009. Development and evolution of insect pigmentation: genetic mechanisms and the potential consequences of pleiotropy. Semin. Cell Dev. Biol. 20, 65–71.
Wittkopp, P.J., Carroll, S.B., Kopp, A., 2003. Evolution in black and white: genetic control of pigment patterns in *Drosophila*. Trends Genet. 19, 495–504.
Wu, S.Y., Tong, X.L., Peng, C.X., Xiong, G., Lu, K.P., Hu, H., Tan, D., Li, C.L., Han, M.J., Lu, C., Dai, F.Y., 2016. Comparative analysis of the integument transcriptomes of the black dilute mutant and the wild-type silkworm *Bombyx mori*. Sci. Rep. UK 6.
Xia, Q., Cheng, D., Duan, J., Wang, G., Cheng, T., Zha, X., Liu, C., Zhao, P., Dai, F., Zhang, Z., He, N., Zhang, L., Xiang, Z., 2007. Microarray-based gene expression profiles in multiple tissues of the domesticated silkworm, Bombyx mori. Genome Biol. 8, R162.
Xiang, Z., 1995. Genetics and Breeding of the Silkworm. CHN: Chinese Agriculture Press, Beijing.
Xiong, G., Tong, X., Gai, T., Li, C., Qiao, L., Monteiro, A., Hu, H., Han, M., Ding, X., Wu, S., Xiang, Z., Lu, C., Dai, F., 2017. Body shape and coloration of silkworm larvae are influenced by a novel cuticular protein. Genetics 207, 1053–1066.
Yoda, S., Yamaguchi, J., Mita, K., Yamamoto, K., Banno, Y., Ando, T., Daimon, T., Fujiwara, H., 2014. The transcription factor Apontic-like controls diverse colouration pattern in caterpillars. Nat. Commun. 5, 4936.
Zhang, J., Zhu, K.Y., 2006. Characterization of a chitin synthase cDNA and its increased mRNA level associated with decreased chitin synthesis in Anopheles quadrimaculatus exposed to diflubenzuron. Insect Biochem. Mol. Biol. 36, 712–725.